On the statistical significance of foreshock sequences in Southern California

M. P. A. van den Ende*[1] and J.-P. Ampuero[1,2]

[1]Université Côte d'Azur, IRD, CNRS, Observatoire de la Côte d'Azur, Géoazur, France

[2]Seismological Laboratory, California Institute of Technology, Pasadena, CA, USA

Abstract

Earthquake foreshocks may provide information that is critical to short-term earthquake forecasting. However, foreshocks are far from ubiquitously observed, which makes the interpretation of ongoing seismic sequences problematic. Based on a statistical analysis, Trugman and Ross (2019) suggested that as much as 72 % of all mainshocks in Southern California are preceded by foreshock sequences. In this study, we re-assess the analysis of Trugman and Ross (2019), and we evaluate the impact of the assumptions made by these authors. Using an alternative statistical approach, we find that only 15 out of 46 mainshocks (33 %) are preceded by significantly elevated seismicity rates. When accounting for temporal fluctuations in the background seismicity, only 18 % of the analysed foreshock sequences remain unexplained by the background seismicity. These results imply that even in a highly complete earthquake catalogue, the majority of earthquakes do not exhibit detectable foreshock sequences.

1 Introduction

Prior to large earthquakes, precursory signals, such as accelerating aseismic creep (see Roeloffs, 2006) and elevated tremor and foreshock activity (Dodge et al., 1996; Jones and Molnar, 1979; Marsan and Enescu, 2012), may be recorded by GPS and seismic stations. However, the majority of observations of transient creep and elevated seismicity have only been identified as precursory signals in hindsight. Without prior knowledge of the timing and location of the mainshock, unambiguous identification of earthquake precursors is enigmatic. While it has been argued that some, if not most large earthquakes are preceded by detectable foreshock sequences (Bouchon et al., 2013), (locally) elevated seismicity rates do not uniquely signify the advent of an earthquake, as many of these excursions simply return to the (average) background seismicity rate. These observations prohibit the utilisation of seismicity rates in earthquake forecasting attempts to-date.

Recently, Trugman and Ross (2019, T&R from here on) performed an in-depth statistical analysis of the seismicity rates preceding 46 mainshock events in Southern California employing a highly

*Corresponding author: martijn.vandenende@geoazur.unice.fr

complete earthquake catalogue (the QTM catalogue; Ross et al., 2019). By comparing short-term seismicity rates with the background rate over one year prior to a selected mainshock, T&R concluded that over 70 % of all analysed mainshocks were preceded by a statistically significant increase in seismicity rates. These authors further alluded to the possibility that in practically all cases foreshock sequences may be detected, provided by that the earthquake catalogue is sufficiently complete. If this claim holds true, this has the implication that the nucleation process of (large) earthquakes emits detectable information with potential application in short-term earthquake forecasting. However, the reported results do not immediately illuminate the significance of elevated seismicity rates when taking into perspective the ubiquitous fluctuations in the background seismicity rate: if similar elevations in the seismicity rate are observed at random 70 % of the time, the presence of a foreshock sequence may simply be due to random chance.

In this work, we revisit the analysis of T&R to assess the significance of their findings, additionally taking into account fluctuations in the background seismicity rate. We first describe the procedure to reproduce the results reported by these authors and comment on some of the assumptions made in this procedure. We subsequently propose an alternative approach that relaxes these assumptions, and we re-assess the statistical significance and interpretation of elevated seismicity rates prior to large earthquakes. We find that the number of mainshocks preceded by statistically significant foreshock activity (taken in a broad sense) is substantially less than reported by T&R (33 % versus 70 %, respectively). Nonetheless, this observed number of foreshock sequences is not fully attributable to random fluctuations in the background seismicity rates (happening 15 % of the time), which suggests that in some cases elevated seismicity rates are uniquely associated with mainshock events.

2 Statistical methods

2.1 Reproducing the results of Trugman and Ross (2019)

To set a reference, we begin by reproducing the results reported by Trugman and Ross (2019). Although the approach taken by these authors has been described extensively in their main manuscript and in their supplementary information, certain details of the procedure were omitted for brevity. Below we briefly describe the procedure including these details, based on personal communication with D. Trugman.

Firstly, we extract the 46 mainshock events as identified by T&R from the QTM catalogue (Ross et al., 2019). For each of these events, we collect all earthquakes that are located within a rectangular box extending ±10 km around the mainshock with no depth cut-off. We then compute the interevent time (IET) between each pair of subsequent earthquakes that occurred within 380 days and up to 20 days prior to each mainshock. A time window of 20 days prior to the main event is excluded to avoid bias of the estimation of the background rate by potential foreshock activity. The distribution of IET tends to follow a gamma distribution, of which the probability density function ρ is defined as:

$$\rho(\tau;\gamma,\mu) = \frac{\tau^{\gamma-1}e^{-\mu\tau}}{\mu^{-\gamma}\Gamma(\gamma)} \tag{1}$$

where τ is the interevent time, γ the shape parameter, μ the background rate, and $\Gamma(\gamma)$ the gamma function. The ratio of independent events over the total number of events (including clustered events) is represented by the shape parameter γ. A shape parameter of $\gamma = 1$ indicates that all events are in the catalogue are mutually independent, and accordingly Eqn. (1) reduces to the exponential distribution (associated with a Poisson process). By fitting the above gamma distribution to the IETs of events within -380 d $\leq t < -20$ d prior to each individual mainshock, we obtain γ and μ that characterise the background seismicity rate associated with each mainshock event.

Next, T&R assumed a Poisson distribution of observing N_{obs} earthquakes in a given 20-day time interval, of which the probability mass function is defined as:

$$P(N_{obs}) = \frac{1}{N_{obs}!}\lambda^{N_{obs}}e^{-\lambda} \tag{2}$$

where $\lambda = \mu T$, with T being the observation time window of 20 days. The probability of observing at least N_{obs} events over the 20 days preceding the mainshock is given by the survival function:

$$p(N \geq N_{obs}) = 1 - \sum_{n=0}^{N_{obs}-1} \frac{\lambda^n}{n!}e^{-\lambda} \tag{3}$$

Low values of p imply that the number of events in the 20-day window is unlikely to be observed given the background rate μ, and hence are an indication of anomalously high seismicity rates. Following T&R, we adopt a value of $p < 0.01$ as a threshold for the statistical significance of the seismicity rates.

2.2 Alternative approach based on random sampling

A key assumption in the above procedure of estimating the expected 20-day event count (i.e. Eqn. (3)), is that the seismicity rate follows a Poisson distribution. This implicitly requires that each event in the analysed sequence be statistically independent (and accordingly $\gamma = 1$). While this requirement may be met for individual mainshock events, the QTM catalogue contains numerous occasions of (short) aftershock sequences associated with events of magnitude $M_w < 4$ (which are therefore not considered as mainshocks). To estimate the background seismicity rate based on the interevent times does not require special treatment of correlated events (Hainzl et al., 2006), and so the estimates of μ obtained by fitting a gamma distribution are representative (for any $\gamma \leq 1$). On the other hand, to subsequently assess the significance of observing N_{obs} events in a given time-window based on a Poisson survival function, declustering of the earthquake catalogue is essential (e.g. Reasenberg, 1985). To circumvent this, we propose an alternative method below that does not assume Poissonian behaviour.

After fitting the gamma distribution to the IET data (see previous section), we draw N random samples of IET from the resulting probability density function. The total duration Δt of a sequence of N earthquakes is therefore:

$$\Delta t = \sum^{N} \hat{\tau} \tag{4}$$

where $\hat{\tau}$ is a random sample drawn from $\rho(\tau;\gamma,\mu)$ (Eqn. (1)). The number of events that are observed within a 20-day time window T is thus defined as the largest value of N for which $\Delta t \leq T$. Note that each sequence begins with an earthquake at $t = 0$, but that this does not affect the statistics of N. By generating 50 000 realisations of Δt, we obtain a distribution of N, i.e. the distribution of earthquakes occurring in a time window of 20 days based on the measured background seismicity rate μ and shape factor γ. Since Δt results from the summation of random samples drawn from a gamma distribution, we make use of the following property (for a proof, see Appendix A):

$$\sum^{N} \hat{\tau} \sim \rho(\Delta t; N\gamma, \mu) \tag{5}$$

i.e. the summation of samples drawn from a gamma distribution itself follows a gamma distribution of which the shape factor γ is multiplied by N. By introducing the criterion that $\Delta t \approx T = \text{const.}$, it is to be expected that N also follows a gamma distribution (which we will demonstrate numerically in the next section).

Under the assumption that N is gamma distributed, we fit a gamma distribution to the random realisations of N, and calculate the probability of observing at least N_{obs} events in a 20-day window from the corresponding survival function. A probability lower than a threshold of 0.01 signifies an elevated seismicity rate that is not expected based on the background seismicity rate. We then compare the p-values obtained following this approach with those obtained by T&R under the assumption of Poissonian behaviour.

3 Results

The IET distributions and the corresponding fit with the gamma distribution for all 46 events is given in Supplementary Figure S1. The values of γ and μ obtained from the fitting procedure, and their comparison with those of Trugman and Ross (2019), are reported in Supplementary Table S1. Examples of four selected events are given in Fig. 1. Throughout the remainder of this work, the same four selected events are considered. In most cases, the quality of the fit is good if the number of events in the catalogue is sufficient to produce robust statistics, indicating that the IET statistics are indeed captured well by a gamma distribution. The seismicity rate parameters μ inferred in this study are overall similar to those estimated by T&R (though our μ-values are systematically higher), verifying the first step in our approach.

Based on random sampling of the best-fit gamma distributions, distributions of the 20-day event counts (N) are obtained (see Fig. 2). As discussed in Section 2.2, N itself follows a gamma distribution, which is in strong contrast to the Poisson distribution assumed by T&R. As can be clearly seen in Fig. 2, the probability density given by a Poisson distribution rapidly decays towards zero with increasing N, often well before the median value of N is reached. This has tremendous implications for the resulting p-value estimates, as the integral over the tail of the Poissonian N-distribution is effectively zero for any range of observed N.

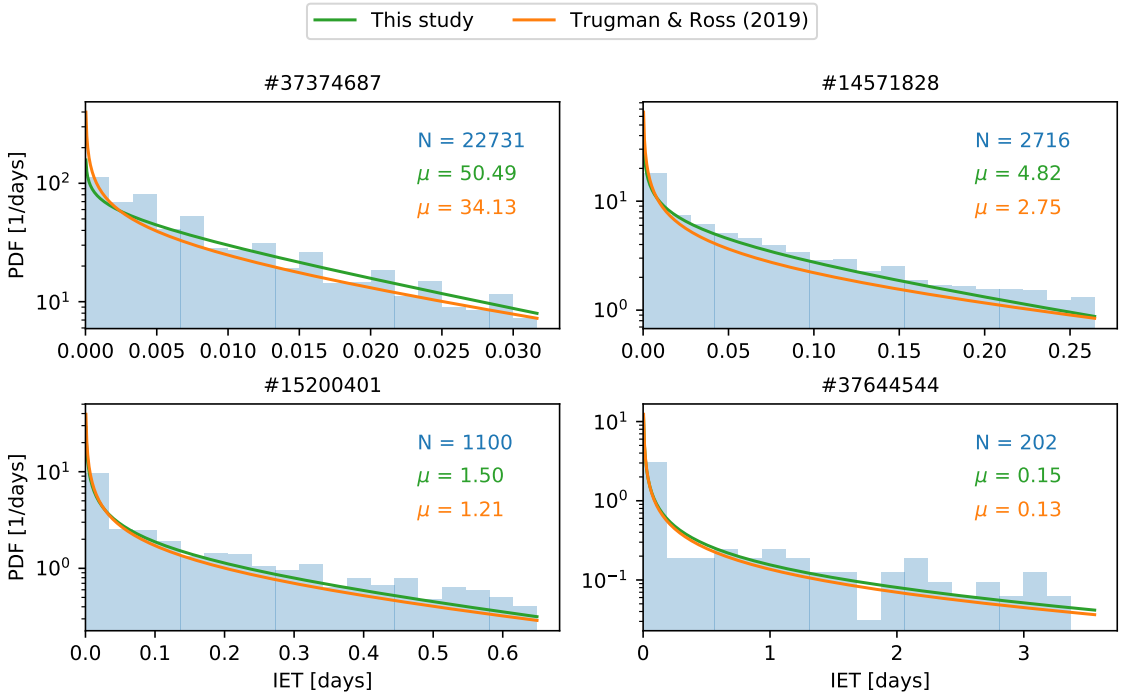

Figure 1: Interevent time (IET) distributions of four selected mainshock events (indicated in each panel's title), along with the best-fit gamma distributions (this study and Trugman and Ross (2019)). The total number of events N and the inferred background rate μ (events per day) are as indicated in each panel.

To highlight this, we plot the probability curves (i.e. survival functions) of observing at least N events in a 20-day window of the four selected mainshock events (Fig. 3). While the survival functions based on the gamma distributions plotted in Fig. 2 remain well above the significance threshold in three out of four cases, the survival function based on the Poisson distribution (as adopted by T&R) sharply drops to zero in all selected cases, suggesting that all the observed earthquake sequences cannot be attributed to the background seismicity (i.e. $p < 0.01$ in all cases). In our analysis, only 15 out of 46 mainshocks (32.6 %) are characterised by elevated seismicity rates that are statistically significant ($p < 0.01$). When performing an identical analysis of the Southern California Seismicity Network (SCSN) catalogue (Hutton et al., 2010), we find that 9 out of 45 mainshocks (20 %) exhibit significantly elevated seismicity rates prior to the main event.

4 Discussion

4.1 Temporal fluctuations of background seismicity

While the analysis of the seismicity over 20 days prior to each mainshock has indicated that 33 % of all mainshocks exhibit significantly elevated seismicity rates, it is at this point not known whether this enhanced seismicity is uniquely associated to the mainshock event, or whether similar excursions

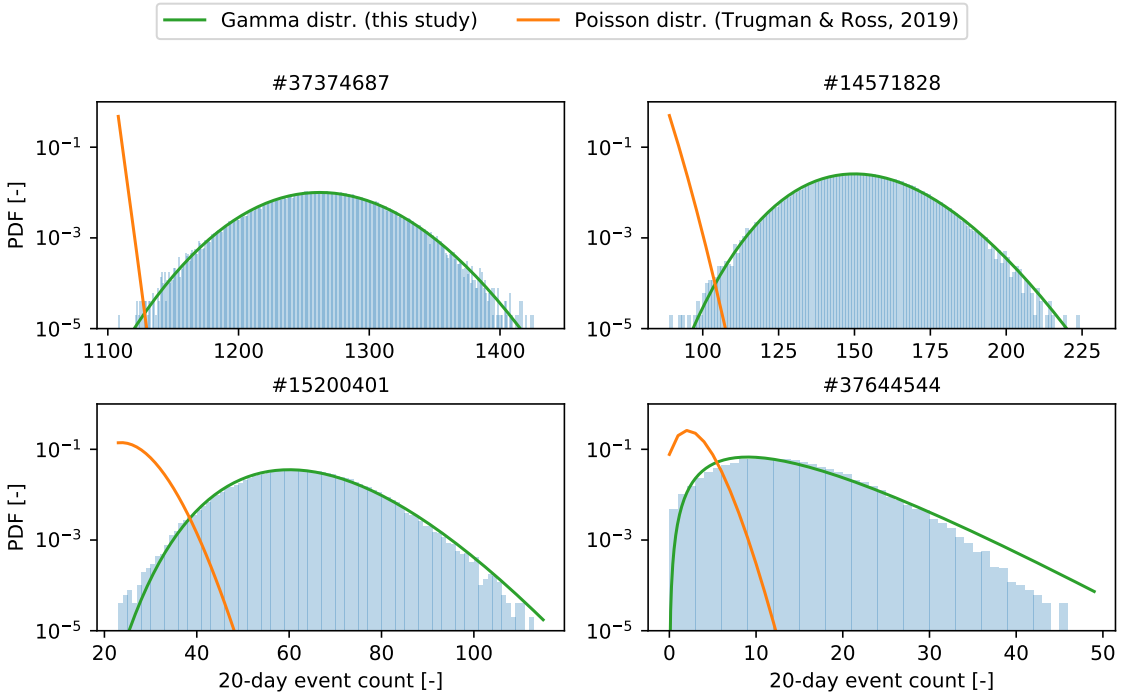

Figure 2: Distributions of the number of events (N) observed in a 20-day time window of four selected mainshock event (indicated in each panel title), based on random sampling of the IET gamma distributions. N itself follows a gamma distribution, as indicated by the green line in each panel. The Poisson distribution as assumed by Trugman and Ross (2019) is indicated by the orange line.

from the background seismicity occur also in the absence of mainshock events. These excursions are expected to occur either in the form of swarm activity, or as aftershocks of smaller ($M_w < 4$) earthquakes. To this end, we compute the p-value at a given moment in time by sampling the gamma distribution (as described in Section 2.2) over a 20-day sliding window. This sliding window traverses the full duration of 380 d prior to the mainshock with strides of 1 d, so that the seismicity rate over this period is continuously evaluated relative to the (average) background seismicity rate. As before, we consider a p-value less than 0.01 to define a statistically significant increase in seismicity. The result of this analysis for four selected mainshocks is presented in Fig. 4 (the analysis of all 46 mainshocks is given in Supplementary Figure S3).

The variability in the background seismicity rate can be quantified by computing the fraction of time-windows for which $p < 0.01$ for all mainshock events combined. Doing so gives a fraction of 15.2 %, i.e. at any given moment in time there is a 15.2 % probability of observing an elevated seismicity rate. When comparing this value with the estimation that 33 % of all mainshocks are preceded by significantly elevated seismicity rates, we conclude that about half of these "foreshock sequences" would have been expected purely on the basis of a fluctuating background rate. This leaves only a small number of mainshocks (about 8) in the catalogue that are truly preceded by a foreshock sequence associated with the nucleation process of the earthquake.

4.2 Statistical significance of foreshock activity

When relaxing the assumption of Poissonian behaviour, and when considering the temporal fluctuations in the background seismicity rate, only a minority of mainshock events are preceded by foreshock sequences. This is in strong contrast to the 70 % estimated by T&R, who further alluded to the possibility of detecting more foreshock sequences in catalogues of higher completeness. While an identical analysis of the less complete SCSN catalogue has yielded a somewhat lower proportion of mainshocks preceded by significantly elevated seismicity rates (20 % for SCSN versus 33 % for QTM), this difference is unlikely to be statistically robust given the small number of mainshocks considered, and so our results are inconclusive regarding the importance of catalogue completeness. However, our findings are within the (wide) range of estimates given by previous studies (e.g. Abercrombie and Mori, 1996; Chen and Shearer, 2016; Jones and Molnar, 1976; Reasenberg, 1999), providing some confidence in the approach adopted in this study. The quantitative differences between this study and that of T&R can also be seen qualitatively by considering the seismicity over the full 380 d preceding the mainshock. For instance, events # 37374687 and # 37644544 (top and bottom rows in Fig. 3) seem to exhibit seismicity rates over the 20 days immediately prior to the mainshock that are not unusually high considering the preceding 380 days. It is therefore not intuitive to imagine a p-value that is practically zero, as given by the Poissonian survival function.

On the other hand, event # 14571828 (second row in Fig. 3) does seem to exhibit a short burst of seismic activity the same day as the mainshock event. Unfortunately, owing to the extent of the time-window over which the p-value is considered (20 days), this clear burst of activity is of insufficient duration to exceed the p-value threshold. Therefore, to decide whether or not a particular mainshock exhibits significant foreshock activity, visual inspection of the catalogue is recommended, rather than to rely purely on the computed p-values. Alternatively, other seismological metrics such as a changing b-value could be considered to alleviate the effect of a fixed temporal window (Gulia and Wiemer, 2019).

5 Conclusions

In this study, we re-assessed the significance of foreshock activity in Southern California, following the analysis of Trugman and Ross (2019). While the characterisation of the background seismicity rate based on the interevent time (IET) method is robust, the subsequent assumption that all earthquakes in the catalogue are statistically independent (and may therefore be described by a Poisson distribution) is overly restrictive. Consequently, the number of events expected to be observed in a 20-day time interval directly prior to a mainshock event is severely underestimated, and the number of mainshocks exhibiting statistically significant foreshock activity overestimated. Based on a random sampling approach that does not invoke the assumption of Poissonian behaviour, we estimate that only 33 % (15 out of 46) of all mainshocks are preceded by elevated seismicity rates, while about half of that fraction is a-priori anticipated based on the ubiquitous fluctuations in the background seismicity rate. In other words, we expect that only about 15 % of all mainshocks exhibit a foreshock sequence uniquely associated with the earthquake preparation process.

6 Appendix A: proof of Eqn. (5)

Suppose X and Y are independent random variables following a gamma distribution, with probability density functions (PDFs) $\rho_X(x;\gamma_x,\mu)$ and $\rho_Y(y;\gamma_y,\mu)$, respectively. The PDF of the sum of these variables ($Z = X + Y$) is found by convolving ρ_X with ρ_Y, i.e.:

$$\rho_Z(z) = \int_{-\infty}^{+\infty} \rho_X(x)\rho_Y(z-x)\mathrm{d}x \tag{6}$$

For $x, y \geq 0$ (and consequently $z - x \geq 0$), the PDFs are non-zero only over the range $[0, z]$, which defines the upper and lower limits of the integration. Substituting the definition of the gamma distribution PDF (see Eqn. (1)), we get:

$$\begin{aligned}\rho_Z(z) &= \int_0^z \frac{x^{\gamma_x-1}e^{-\mu x}}{\mu^{-\gamma_x}\Gamma(\gamma_x)} \frac{(z-x)^{\gamma_y-1}\,e^{-\mu(z-x)}}{\mu^{-\gamma_y}\Gamma(\gamma_y)}\mathrm{d}x \\ &= \frac{e^{-\mu z}}{\mu^{-[\gamma_x+\gamma_y]}} \int_0^z \frac{x^{\gamma_x-1}\,(z-x)^{\gamma_y-1}}{\Gamma(\gamma_x)\Gamma(\gamma_y)}\mathrm{d}x\end{aligned} \tag{7}$$

A change of variables $x = zt$ gives:

$$\rho_Z(z) = \frac{e^{-\mu z}}{\mu^{-[\gamma_x+\gamma_y]}} z^{\gamma_x+\gamma_y-1} \int_0^1 \frac{t^{\gamma_x-1}\,(1-t)^{\gamma_y-1}}{\Gamma(\gamma_x)\Gamma(\gamma_y)}\mathrm{d}t \tag{8}$$

Finally, we recognise the emergence of the beta distribution, defined as:

$$B(t;\alpha,\beta) = \Gamma(\alpha+\beta)\frac{t^{\alpha-1}\,(1-t)^{\beta-1}}{\Gamma(\alpha)\Gamma(\beta)} \tag{9}$$

which, upon substitution, gives:

$$\begin{aligned}\rho_Z(z) &= \frac{e^{-\mu z}}{\mu^{-[\gamma_x+\gamma_y]}} \frac{z^{\gamma_x+\gamma_y-1}}{\Gamma(\gamma_x+\gamma_y)} \int_0^1 B(t;\gamma_x,\gamma_y)\mathrm{d}t \\ &= \frac{e^{-\mu z}}{\mu^{-[\gamma_x+\gamma_y]}} \frac{z^{\gamma_x+\gamma_y-1}}{\Gamma(\gamma_x+\gamma_y)} \\ &= \frac{z^{\gamma_z-1}e^{-\mu z}}{\mu^{-\gamma_z}\Gamma(\gamma_z)}\end{aligned} \tag{10}$$

In other words, the sum of two gamma distributed variables produces new gamma distributed variable, with shape parameter $\gamma_z = \gamma_x + \gamma_y$. Taking $\gamma_x = \gamma_y = \gamma$, the sum over N gamma distributed variables yields a gamma distributed variable with shape parameter $N\gamma$.

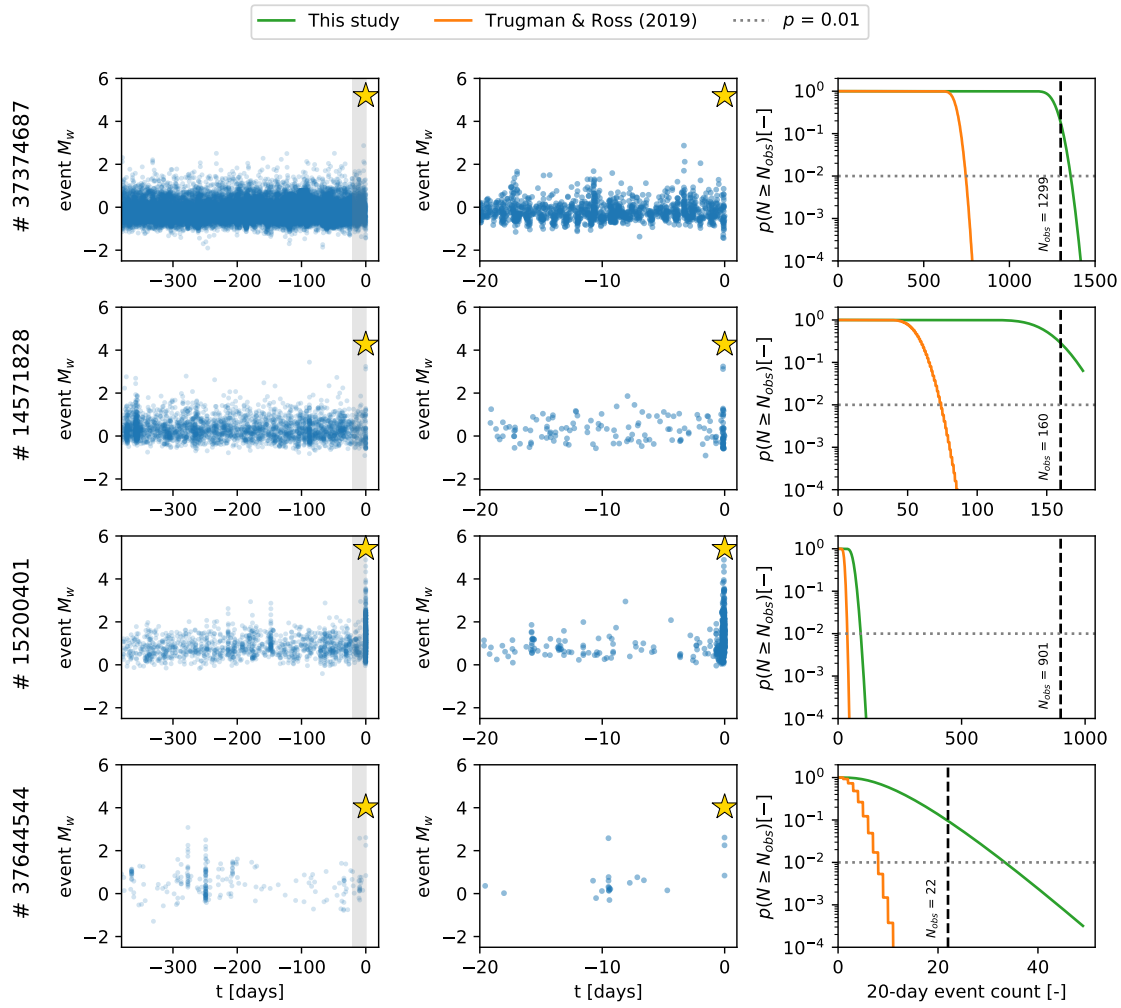

Figure 3: Synthesis of p-value estimates of four selected mainshock events. Left and middle panels: temporal record of earthquake occurrences from 380 d (left) and 20 d (middle) prior to the mainshock. The mainshock is indicated by the yellow star. Right panels: probability curves of observing at least N events in a 20-day window, compared with the number of events observed 20 d prior to the mainshock (N_{obs}). The present analysis based on random sampling of the gamma distribution is indicated by the green line, the Poisson survival function based on the rate parameter μ estimated by Trugman and Ross (2019) is indicated by the orange line. The significance threshold of 0.01 is represented by the horizontal dotted line.

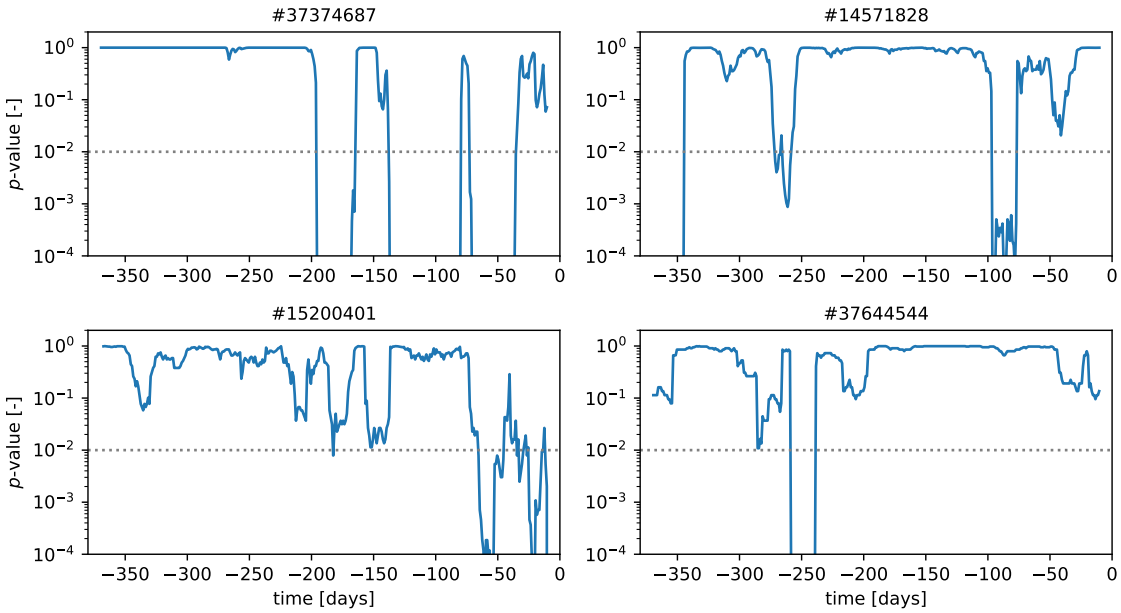

Figure 4: Estimated p-values for the 380 days prior to four selected mainshocks, computed within a sliding 20-day window. For reference, the significance threshold of 0.01 is indicated by the dotted line.

References

Abercrombie, R.E., Mori, J., 1996. Occurrence patterns of foreshocks to large earthquakes in the western United States. Nature 381, 303–307. URL: https://www.nature.com/articles/381303a0, doi:10.1038/381303a0.

Bouchon, M., Durand, V., Marsan, D., Karabulut, H., Schmittbuhl, J., 2013. The long precursory phase of most large interplate earthquakes. Nature Geoscience 6, 299–302. URL: http://www.nature.com/articles/ngeo1770, doi:10.1038/ngeo1770.

Chen, X., Shearer, P.M., 2016. Analysis of Foreshock Sequences in California and Implications for Earthquake Triggering. Pure and Applied Geophysics 173, 133–152. URL: https://doi.org/10.1007/s00024-015-1103-0, doi:10.1007/s00024-015-1103-0.

Dodge, D.A., Beroza, G.C., Ellsworth, W.L., 1996. Detailed observations of California foreshock sequences: Implications for the earthquake initiation process. Journal of Geophysical Research: Solid Earth 101, 22371–22392. URL: http://doi.wiley.com/10.1029/96JB02269, doi:10.1029/96JB02269.

Gulia, L., Wiemer, S., 2019. Real-time discrimination of earthquake foreshocks and aftershocks. Nature 574, 193–199. URL: https://www.nature.com/articles/s41586-019-1606-4, doi:10.1038/s41586-019-1606-4.

Hainzl, S., Scherbaum, F., Beauval, C., 2006. Estimating Background Activity Based on Interevent-Time Distribution. Bulletin of the Seismological Society of America 96, 313–320. URL: https://pubs.geoscienceworld.org/ssa/bssa/article-abstract/96/1/313/146796/estimating-background-activity-based-on-intere doi:10.1785/0120050053.

Hutton, K., Woessner, J., Hauksson, E., 2010. Earthquake Monitoring in Southern California for Seventy-Seven Years (1932–2008)Earthquake Monitoring in Southern California for Seventy-Seven Years (1932–2008). Bulletin of the Seismological Society of America 100, 423–446. URL: https://pubs.geoscienceworld.org/bssa/article/100/2/423/349275/Earthquake-Monitoring-in-Southern-California-for, doi:10.1785/0120090130.

Jones, L., Molnar, P., 1976. Frequency of foreshocks. Nature 262, 677–679. URL: https://www.nature.com/articles/262677a0, doi:10.1038/262677a0.

Jones, L.M., Molnar, P., 1979. Some characteristics of foreshocks and their possible relationship to earthquake prediction and premonitory slip on faults. Journal of Geophysical Research: Solid Earth 84, 3596–3608. URL: http://doi.wiley.com/10.1029/JB084iB07p03596, doi:10.1029/JB084iB07p03596.

Marsan, D., Enescu, B., 2012. Modeling the foreshock sequence prior to the 2011, MW9.0 Tohoku, Japan, earthquake. Journal of Geophysical Research: Solid Earth 117. URL: https://agupubs.onlinelibrary.wiley.com/doi/full/10.1029/2011JB009039, doi:10.1029/2011JB009039.

Reasenberg, P., 1985. Second-order moment of central California seismicity, 1969–1982. Journal of Geophysical Research: Solid Earth 90, 5479–5495. URL: https://agupubs.onlinelibrary.wiley.com/doi/abs/10.1029/JB090iB07p05479, doi:10.1029/JB090iB07p05479.

Reasenberg, P.A., 1999. Foreshock occurrence before large earthquakes. Journal of Geophysical Research: Solid Earth 104, 4755–4768. URL: https://agupubs.onlinelibrary.wiley.com/doi/abs/10.1029/1998JB900089, doi:10.1029/1998JB900089.

Roeloffs, E.A., 2006. EVIDENCE FOR ASEISMIC DEFORMATION RATE CHANGES PRIOR TO EARTHQUAKES. Annual Review of Earth and Planetary Sciences 34, 591–627. URL: http://www.annualreviews.org/doi/10.1146/annurev.earth.34.031405.124947, doi:10.1146/annurev.earth.34.031405.124947.

Ross, Z.E., Trugman, D.T., Hauksson, E., Shearer, P.M., 2019. Searching for hidden earthquakes in Southern California. Science 364, 767–771. URL: https://science.sciencemag.org/content/364/6442/767, doi:10.1126/science.aaw6888.

Trugman, D.T., Ross, Z.E., 2019. Pervasive Foreshock Activity Across Southern California. Geophysical Research Letters 0. URL: https://agupubs.onlinelibrary.wiley.com/doi/full/10.1029/2019GL083725, doi:10.1029/2019GL083725.

7 Supplements

7.1 Supplementary Figure S1: IET distributions

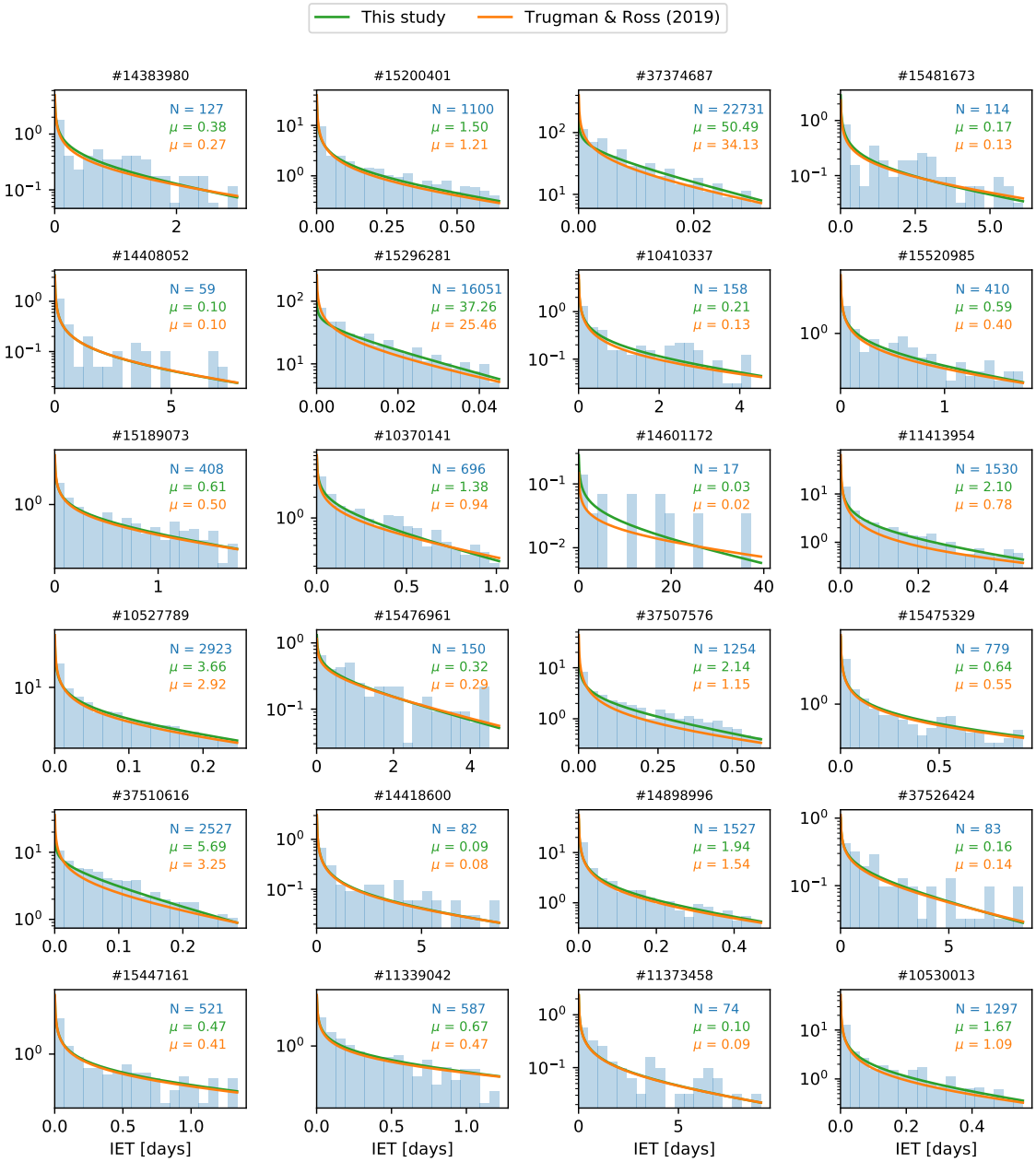

Figure 5: Interevent time (IET) distributions for each mainshock, along with the best-fit gamma distributions (this study and Trugman and Ross (2019)). The total number of events N and the inferred background rate μ (events per day) are as indicated in each panel.

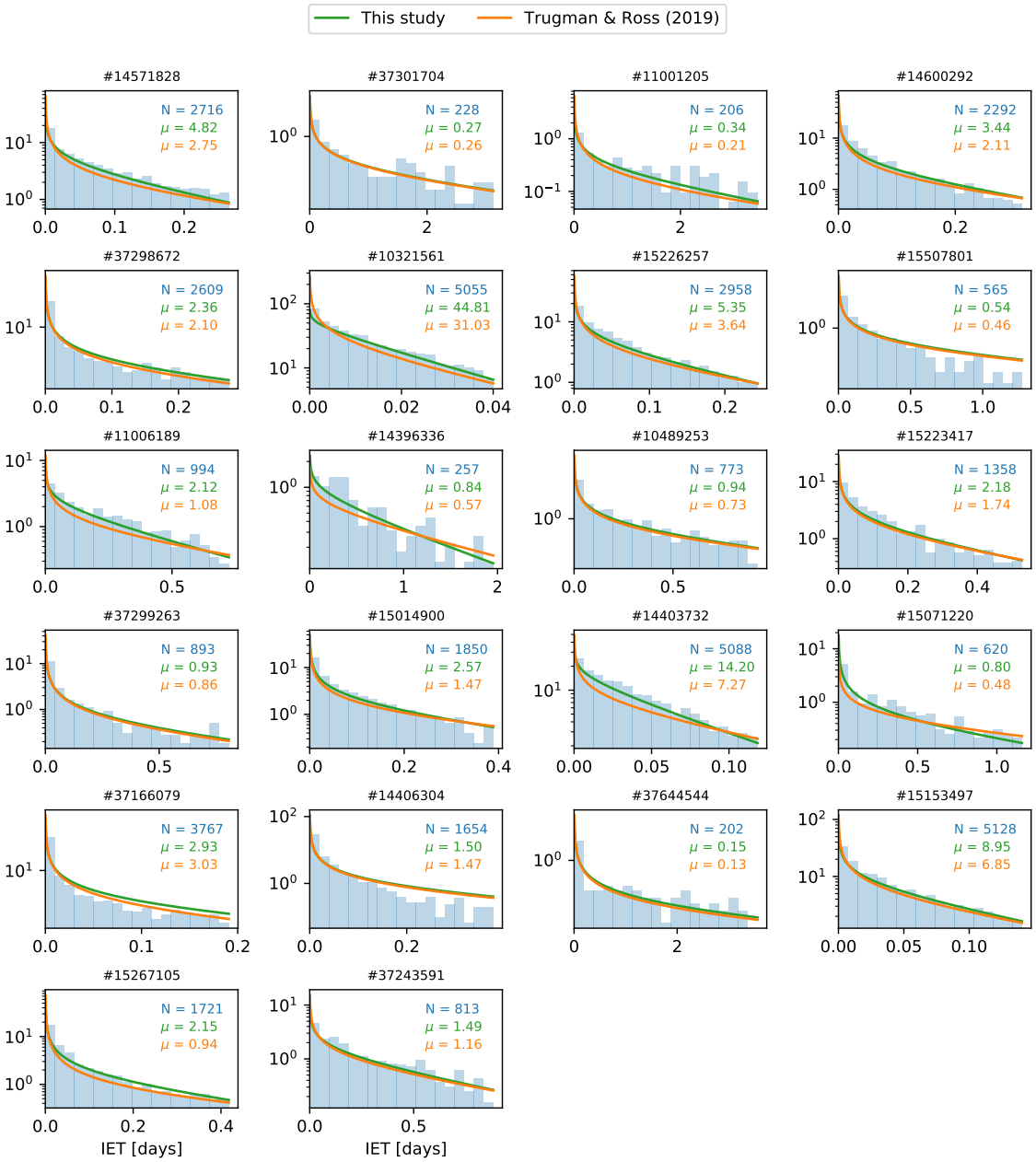

Figure 6: (continued)

7.2 Supplementary Figure S2: seismicity rate distributions

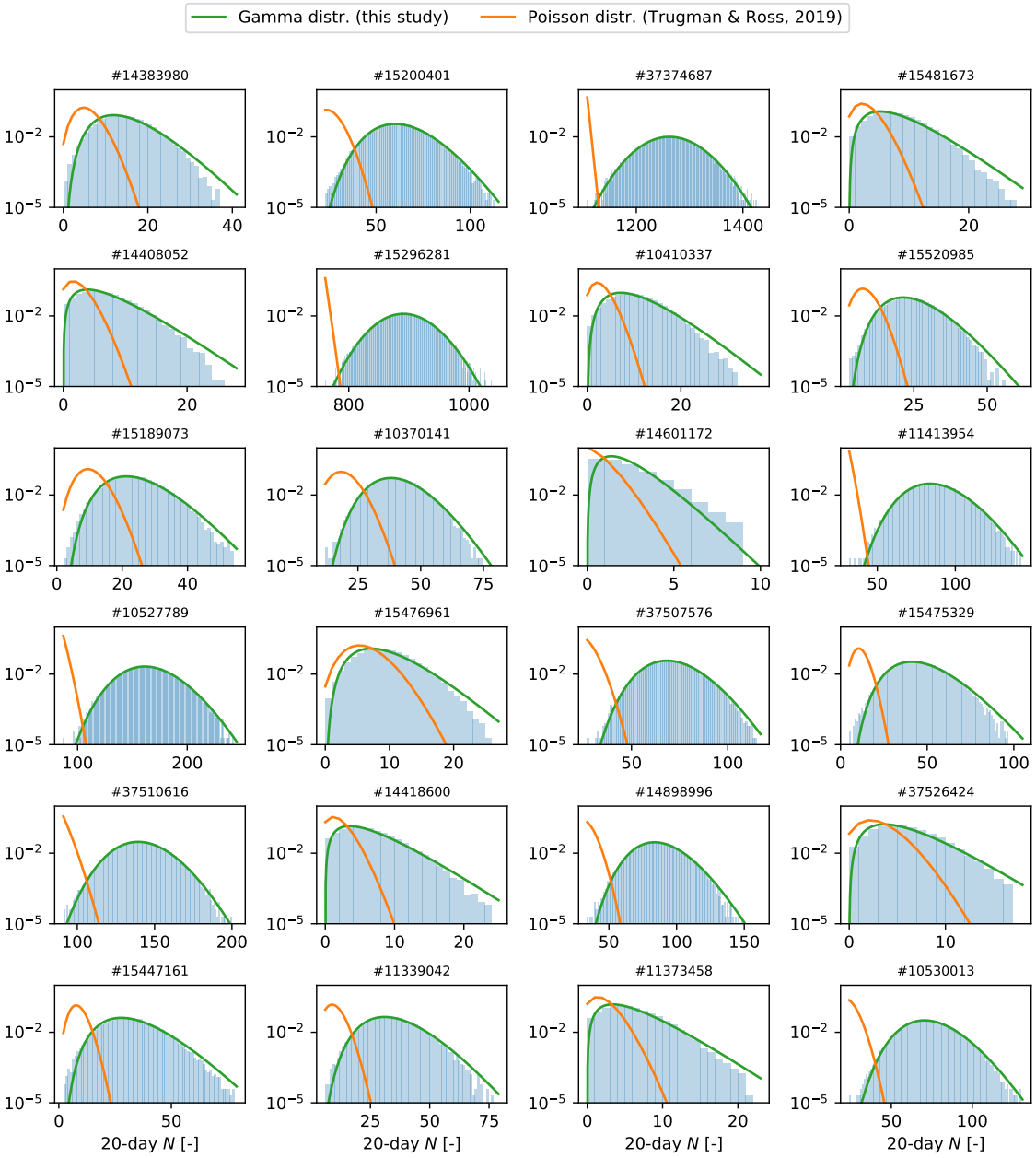

Figure 7: Distributions of the number of events (N) observed in a 20-day time window, based on random sampling of the IET gamma distributions. N itself follows a gamma distribution, as indicated by the red line in each panel. The Poisson distribution as assumed by Trugman and Ross (2019) is indicated by the black dashed line.

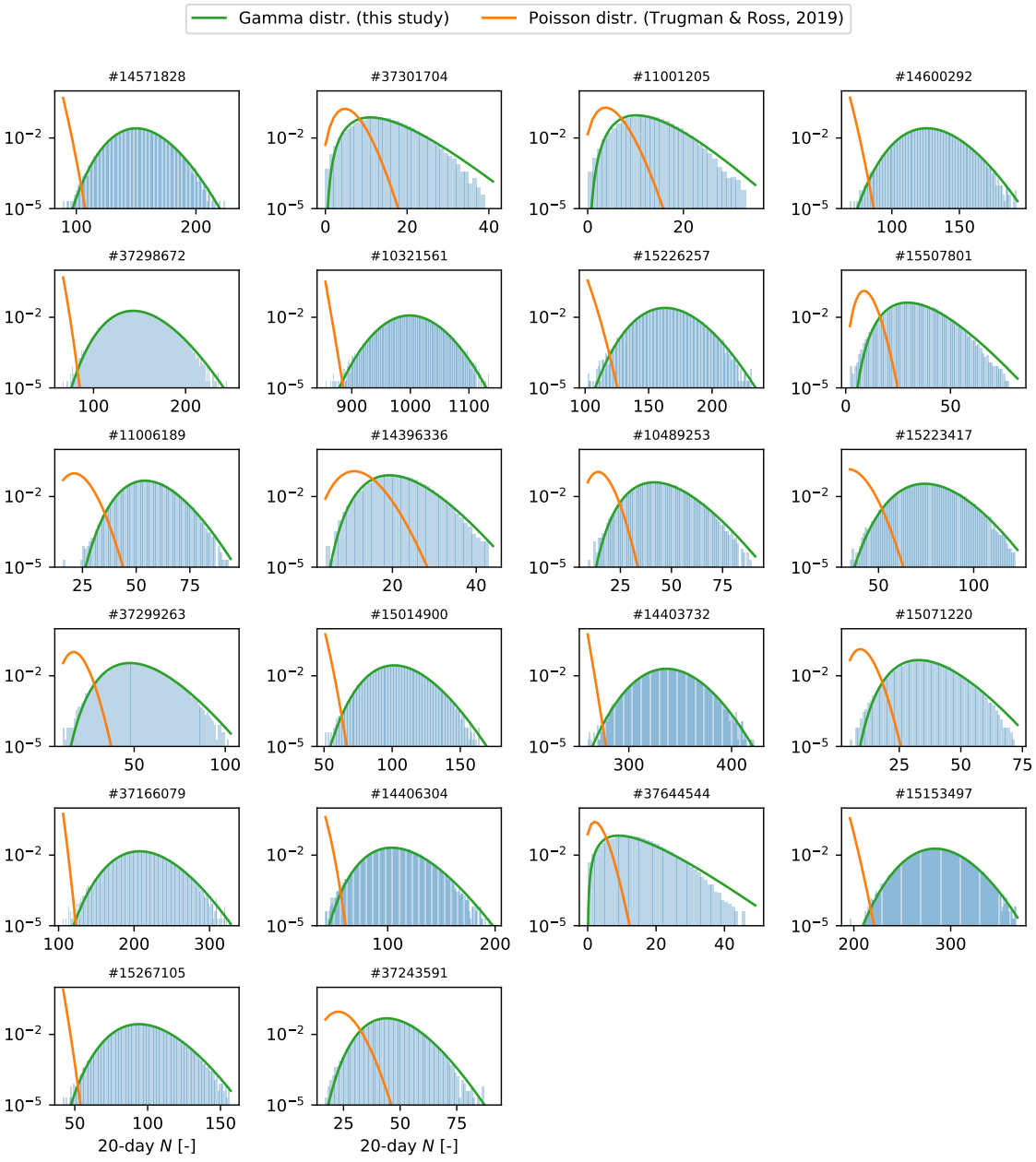

Figure 8: (continued)

7.3 Supplementary Figure S3: temporal fluctuations of the p-value

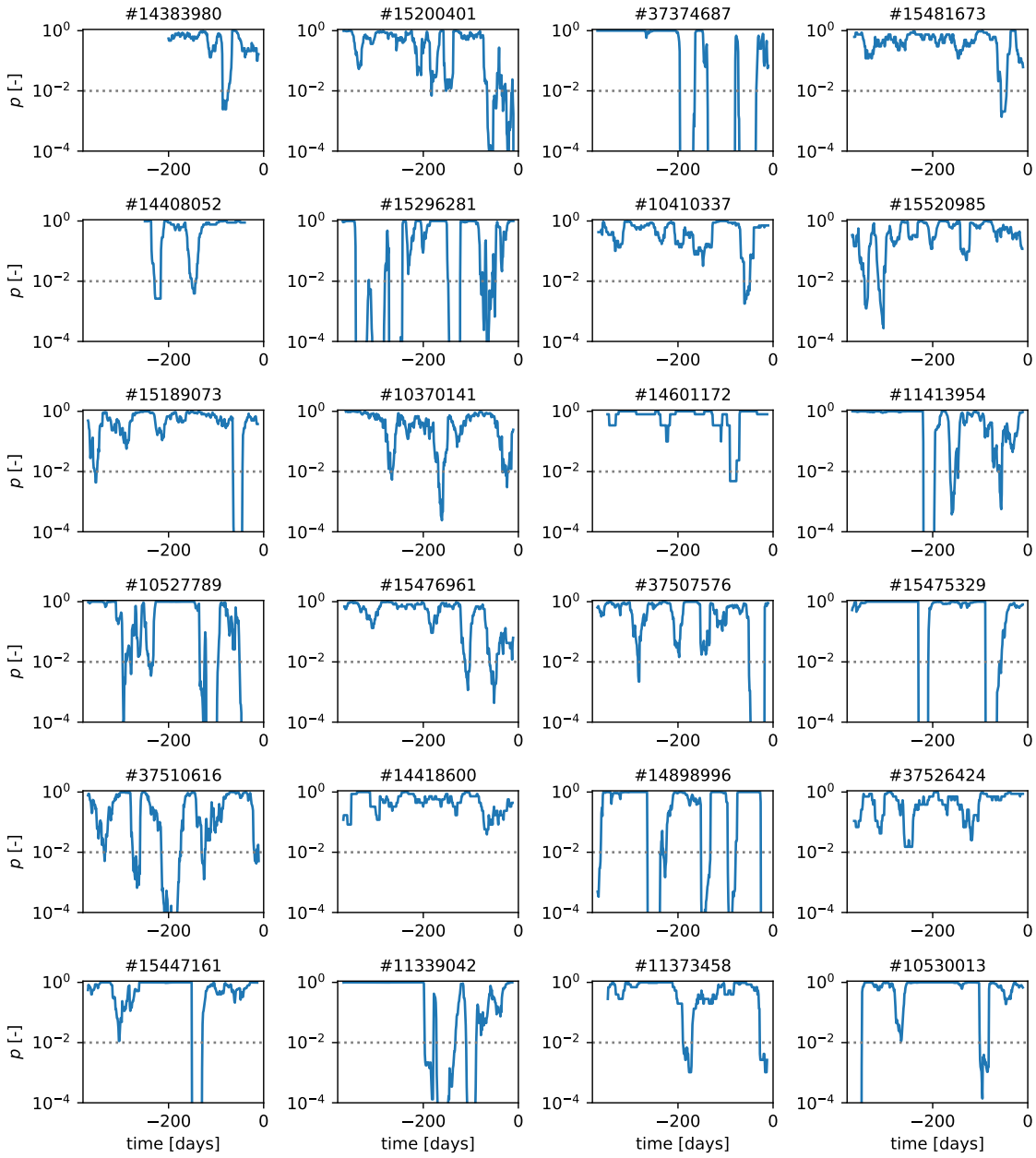

Figure 9: Temporal evolution of the p-value over 380 d prior to the occurrence of each mainshock. A value of $p < 0.01$ indicates a statistically significant elevation of the seismicity rate beyond the background seismicity rate, which is observed about 15 % of the time.

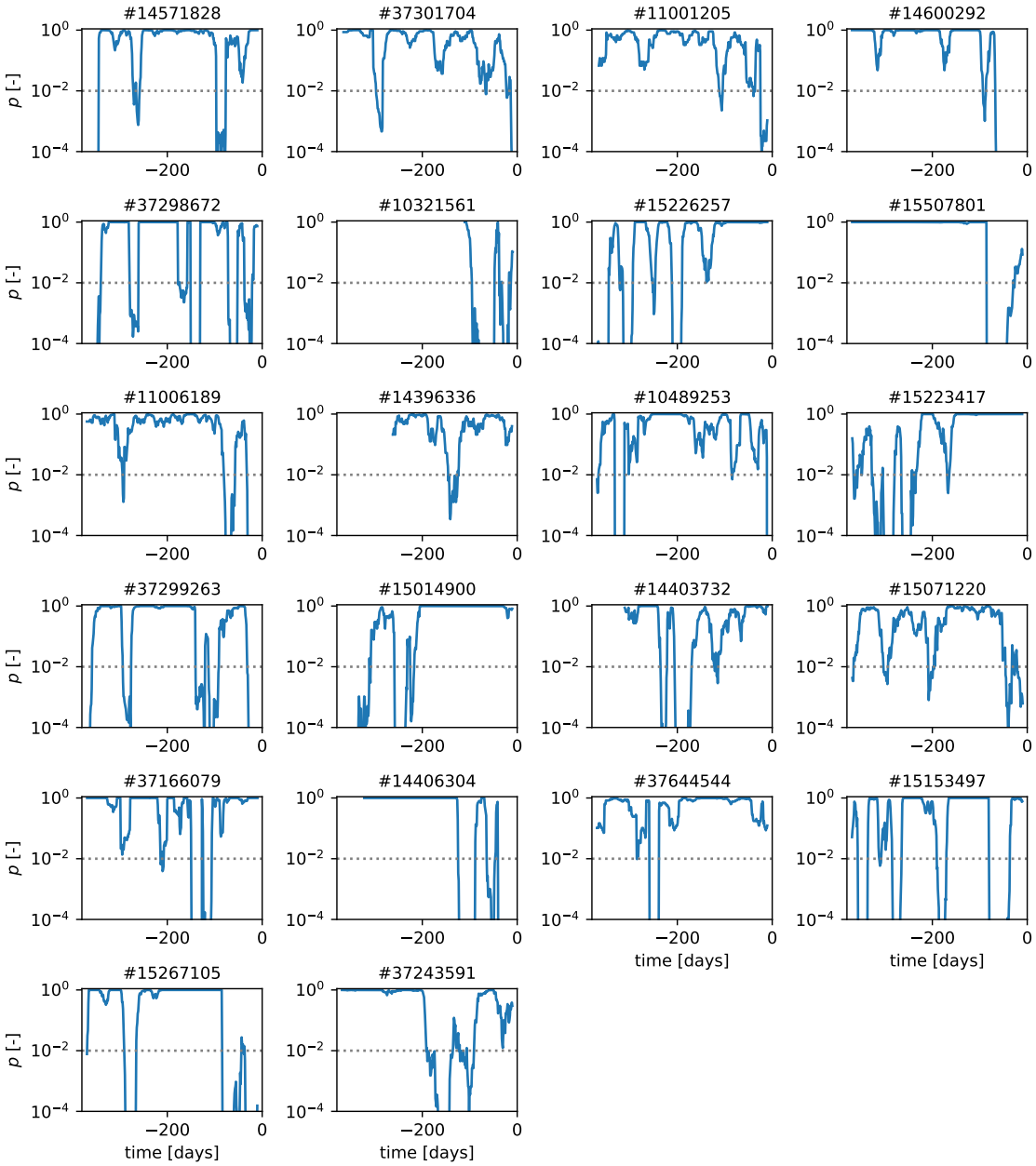

Figure 10: (continued)

7.4 Supplementary Table S1: best-fit gamma distribution parameters

		This study			Trugman and Ross (2019)		
Event ID	M_w	γ [-]	μ [d^{-1}]	p-value	γ [-]	μ [d^{-1}]	p-value
14383980	5.44	0.570	0.381	0.186	0.514	0.265	0.003
15200401	5.41	0.488	1.503	**0.000**	0.402	1.207	0.000
37374687	5.19	0.799	50.485	0.184	0.576	34.129	0.000
15481673	5.09	0.506	0.166	**0.009**	0.523	0.132	0.000
14408052	5.06	0.403	0.103	1.000	0.409	0.103	1.000
15296281	4.70	0.836	37.265	0.974	0.598	25.459	0.000
10410337	4.70	0.464	0.205	0.754	0.371	0.130	0.119
15520985	4.58	0.517	0.590	0.130	0.426	0.403	0.000
15189073	4.46	0.539	0.611	0.655	0.483	0.499	0.014
10370141	4.45	0.698	1.376	0.663	0.641	0.939	0.010
14601172	4.44	0.616	0.031	0.402	0.654	0.016	0.277
11413954	4.43	0.494	2.104	0.871	0.311	0.783	0.000
10527789	4.41	0.450	3.657	**0.000**	0.364	2.919	0.000
15476961	4.40	0.750	0.316	0.052	0.762	0.291	0.007
37507576	4.40	0.615	2.141	0.942	0.393	1.147	0.000
15475329	4.39	0.298	0.644	0.851	0.262	0.549	0.000
37510616	4.39	0.810	5.689	**0.002**	0.599	3.251	0.000
14418600	4.39	0.402	0.092	0.484	0.386	0.083	0.026
14898996	4.37	0.456	1.945	**0.000**	0.391	1.542	0.000
37526424	4.31	0.680	0.162	0.442	0.640	0.136	0.131
15447161	4.30	0.312	0.466	0.957	0.277	0.410	0.020
11339042	4.29	0.408	0.669	0.996	0.352	0.469	0.146
11373458	4.28	0.456	0.100	**0.006**	0.447	0.095	0.000
10530013	4.28	0.463	1.670	0.657	0.355	1.095	0.056
14571828	4.27	0.638	4.822	0.286	0.474	2.746	0.000
37301704	4.25	0.428	0.274	**0.000**	0.411	0.264	0.000
11001205	4.24	0.590	0.342	**0.000**	0.425	0.212	0.000
14600292	4.23	0.541	3.445	**0.000**	0.432	2.109	0.000
37298672	4.19	0.325	2.361	0.827	0.257	2.103	0.000
10321561	4.19	0.896	44.815	0.111	0.621	31.032	0.000
15226257	4.16	0.651	5.351	1.000	0.536	3.642	0.208
15507801	4.16	0.344	0.541	0.094	0.308	0.461	0.000
11006189	4.14	0.766	2.115	**0.000**	0.613	1.081	0.000
14396336	4.14	0.819	0.838	0.436	0.817	0.568	0.110
10489253	4.13	0.436	0.940	**0.000**	0.378	0.732	0.000
15223417	4.13	0.577	2.182	1.000	0.526	1.736	1.000
37299263	4.11	0.373	0.927	**0.000**	0.334	0.861	0.000
15014900	4.11	0.500	2.573	0.860	0.438	1.474	0.000
14403732	4.11	0.841	14.201	0.997	0.692	7.272	0.001
15071220	4.10	0.464	0.801	**0.001**	0.594	0.484	0.073
37166079	4.10	0.279	2.927	1.000	0.202	3.028	0.000
14406304	4.04	0.284	1.504	**0.000**	0.257	1.468	0.000
37644544	4.03	0.272	0.153	0.095	0.224	0.130	0.000
15153497	4.03	0.628	8.950	0.145	0.510	6.853	0.000
15267105	4.02	0.450	2.152	**0.001**	0.306	0.938	0.000
37243591	4.00	0.657	1.489	0.249	0.557	1.160	0.000

Table 1: Overview of inferred gamma distribution parameters γ and μ, and associated p-values. For convenience, our p-value estimates less than the significance threshold of 0.01 are printed in bold face. 15 out of 46 mainshocks are characterised by statistically significant foreshock activity.